

On the stability of laser wakefield electron accelerators in the monoenergetic regime^{a)}

S. P. D. Mangles^{b)} and A. G. R. Thomas

Blackett Laboratory, Imperial College, London SW7 2BZ, United Kingdom

O. Lundh and F. Lindau

Department of Physics, Lund University, PO Box 118, S-22100 Lund, Sweden

M. C. Kaluza^{c)}

Blackett Laboratory, Imperial College, London SW7 2BZ, United Kingdom

A. Persson and C.-G. Wahlström

Department of Physics, Lund University, PO Box 118, S-22100 Lund, Sweden

K. Krushelnick^{d)} and Z. Najmudin

Blackett Laboratory, Imperial College, London SW7 2BZ, United Kingdom

(Received 3 November 2006; accepted 12 December 2006; published online 21 March 2007)

The effects of plasma density and laser energy on the stability of laser produced monoenergetic electron beams are investigated. Fluctuations in the principal beam parameters, namely, electron energy, energy-spread, charge, and pointing, are demonstrated to be minimized at low densities. This improvement in stability is attributed to the reduced time for pulse evolution required before self-injection occurs; i.e., that the pulse is closest to the matched conditions for these densities. It is also observed that electrons are only consistently produced above a density-dependent energy threshold. These observations are consistent with there being a threshold intensity ($a_0 \gtrsim 3$) required for the occurrence of self-injection after accounting for pulse compression. © 2007 American Institute of Physics. [DOI: 10.1063/1.2436481]

I. INTRODUCTION

The production of high-energy electrons from university laboratory scale high-power lasers is currently a very active field of research. By using short, intense laser pulses to drive relativistic plasma waves, it is possible to produce electron beams with high energy, low energy-spread, and low divergence. Such electron beams may have energies at the GeV level, energy-spreads of a few percent, normalized transverse emittance below π mm mrad, and bunch durations below 25 fs.¹⁻⁶

When an intense laser pulse travels through an underdense plasma, it can excite a relativistic plasma wave. The plasma wave is generated by the ponderomotive force of the laser pulse, which expels the mobile electrons from regions of high laser intensity while the heavier ions remain stationary. The resulting space charge distribution is an electron plasma wave traveling with a phase velocity set by the group velocity of the laser pulse. In a sufficiently underdense plasma this velocity is close to the speed of light. The strong electric fields set up by the charge separation are ideal for accelerating electrons. Wakefield generation is most efficient when the pulse dimensions (i.e., waist and pulse length) are on the order of the wavelength of the plasma wave λ_p

$= 2\pi c/\omega_p$, where ω_p is the plasma frequency.

Electrons are produced from these interactions when some of the electrons in the plasma are injected into and trapped by the wave. This can happen if the wakefield amplitude is sufficiently high, i.e., for electric field strengths $E \geq E_0 = m_e c \omega_p / e$. In a one-dimensional (1D) plasma wave, the electrons have longitudinal velocity associated with their wave motion. Hence, to accelerate an electron that is part of the wave motion, it is necessary to turn around an electron moving backwards at $-v_p$, so that it is going forwards at $+v_p$. In 1D, the relativistically correct electric field strength associated with the plasma wave for this to happen is given by $E_{WB} = \sqrt{2(\gamma_p - 1)} \cdot E_0$, where γ_p is the Lorentz factor associated with the phase velocity of the wave v_p .⁷ If too many electrons are dephased from the wave motion, the wave structure can no longer be sustained; i.e., the wave breaks. In a multidimensional plasma wave, the transverse motion of electrons means that it is possible to have electrons that are part of the wave motion, but that also have only a sufficiently small longitudinal velocity at the correct phase of the plasma wave for them to be picked up and accelerated at reduced values of the electric field strength compared to the 1D cold wavebreaking limit.

When the wakefield structure becomes spherical (i.e., a λ_p^3 “bubble”) electrons at the back of the bubble have zero forward momentum in the wave frame $\xi = z - v_p t$, and thus can be injected into the accelerating fields of the bubble. If this process is controlled so that it takes place sufficiently slowly, the wave structure remains intact. Because the injection occurs in a spatially localized position and the electrons

^{a)}Paper UI2 4, Bull. Am. Phys. Soc. 51, 259 (2006).

^{b)}Invited speaker.

^{c)}Current address: Institut für Optik und Quantenelektronik, Friedrich-Schiller-Universität, Max-Wien-Platz 1, 07743 Jena, Germany.

^{d)}Current address: Center for Ultrafast Optical Science and Department of Nuclear Engineering, 6103 ERB-1, 2200 Bonisteel Blvd., University of Michigan, Ann Arbor, Michigan.

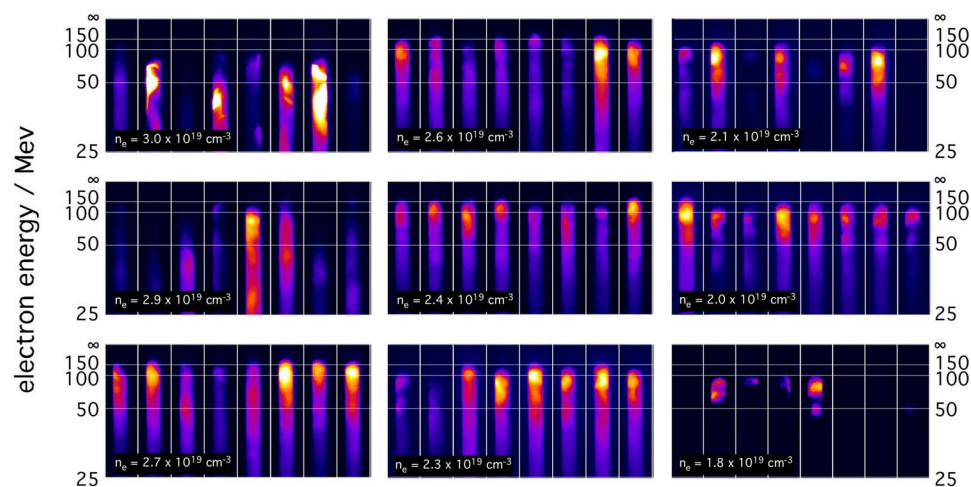


FIG. 1. (Color online) Shot-to-shot variation in electron energy spectrum at various plasma densities. Laser parameters $\mathcal{E}_L \approx 0.7$ J, $\tau_{\text{FWHM}} = 35$ fs. The spectrometer axis is at the top of each image (marked by ∞), electrons are deflected downwards according to their energy. The shots were taken with collimation angle $\approx 0.5^\circ$, giving energy resolution $\approx 10\%$ at 100 MeV and $\approx 2\%$ at 25 MeV. The brightness of the image is proportional to the charge incident on the screen (false color). The color scale for each density is normalized to the peak signal for that density.

are injected with similar energies, after acceleration a narrow-energy-spread electron beam can be produced. Electrons may continue to be injected until the space charge field of the injected bunch becomes comparable to the wakefield strength. At this point beam loading can stop further injection. If the period of injection is significant compared to the dephasing time, then the electrons injected at the beginning of the injection phase will have different energy to those injected later. Even in this case the narrow-energy-spread beams may be produced by phase rotation as the beam overtakes (dephases from) the plasma wave. Though in this case, the monoenergetic peaks are likely to sit on top of a spectrum with greater energy-spread.⁸ For wakefields with an amplitude E_0 , the length over which dephasing occurs is $L_{\text{dp}} = \lambda_p n_c / n_e$. Dephasing also limits the maximum energy gain to $w_{\text{max}} = 2m_e c^2 n_c / n_e$. Here, n_e is the electron density and n_c is the critical density for propagation of the laser (i.e., when $\omega_0 = \omega_p$).

A narrow energy-spread is vital for many applications of these electron beams, such as their use in the generation of short wavelength coherent radiation from free-electron lasers. An equally important property required for applications of these electron beams is stability. It is inconceivable that quality research can be done using laser produced electrons, or radiation generated by them, if the electron beam parameters suffer from large shot-to-shot fluctuations. This paper demonstrates the degree of stability achievable with current laser systems, and discusses how these fluctuations can be reduced. By studying the stability we are able to deduce that pulse evolution is one of the major sources of instability, implying that using matched pulses sufficiently intense to inject electrons will result in further improvements in stability.

II. SHOT-TO-SHOT STABILITY OF LASER-PRODUCED ELECTRON BEAMS

The experiments were performed with the 10 Hz multi-terawatt femtosecond laser at the Lund Laser Centre, a Ti:sapphire system delivering 35-fs pulses of up to 35 TW at a central wavelength of 800 nm. The laser pulses are focused onto the edge of a supersonic gas jet using an $f/10$ off-axis

parabolic mirror. The diffraction limited spot size ($1/e^2$ intensity radius) for a Gaussian beam in this geometry is $w_0 = 5 \mu\text{m}$, with a Rayleigh range of $2Z_R = 2\pi w_0^2 / \lambda = 196 \mu\text{m}$. For a top-hat profile, the full width at half-maximum $w_{\text{FWHM}} = 8.3 \mu\text{m}$, $w_{1/e^2} = 5.4 \mu\text{m}$, with a Rayleigh range of $2Z_R = 215 \mu\text{m}$. Cryogenic cooling of the Ti:sapphire crystal in the final amplifier ensures close to diffraction limited performance. During this experiment, the laser was capable of producing on-target energies up to 0.7 J, corresponding to a peak intensity of $I_0 \approx 4 \times 10^{18} \text{ W cm}^{-2}$, or normalized vector potential of $a_0 \approx 1.4$.

The helium gas jet is capable of producing electron densities in the range $n_e = (0.5 - 5) \times 10^{19} \text{ cm}^{-3}$ (measured off-line using an interferometric technique). The supersonic nozzle produces a 2 mm top-hat radial profile with an approximately 300 μm linear ramp at the edges.

Measurements of the electron energy distribution were performed using a magnetic spectrometer with a scintillating screen (Kodak Lanex) and CCD imaging system as the detector. The magnet in the spectrometer consists of 38 mm diameter circular pole pieces and can produce field strengths up to 0.8 T. For 0.8 T, the spectrometer can measure electron energies $W < 300$ MeV with a few percent resolution when used in conjunction with a steel collimator. Separate measurements of the electron beam profile were made with a second scintillating screen placed between the electron spectrometer and the gas jet. A 12 mm thick aluminum sheet was placed in front of the beam profile monitor to prevent electrons below ≈ 7 MeV reaching the detector. The beam profile monitor was placed at 45° to the laser beam axis to allow imaging at 90° without projection errors.

Figure 1 shows a series of measured electron energy spectra for a range of different plasma densities. The highest density presented ($n_e = 3 \times 10^{19} \text{ cm}^{-3}$) shows a highly unstable spectrum, containing some narrow-energy-spread features. However, these narrow-energy-spread features are superimposed on top of a broad-energy-spread “dark current.” There is also structure in the transverse direction.

As the density is reduced the electron beam becomes more monoenergetic, with the energy spread of the electron bunch becoming narrower. The stability of the electron beam

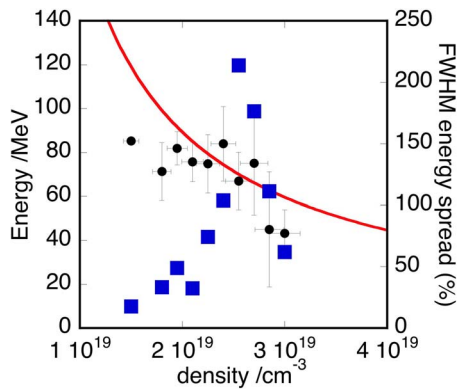


FIG. 2. (Color online) Variation in electron beam energy (circles, left axis) and percent FWHM energy-spread (squares, right axis) with plasma density. The curves shows the linear estimate for maximum energy $w_{\max} = 2m_e c^2(n_e/n_e)$. The error bars on the beam energy represent the standard deviation from the mean value over a series of shots.

is noticeably improved. The ratio of the charge in the monoenergetic peak to the charge in the dark current, also increases as the density decreases. Finally, it is noted that the energy of the electron beam also increases as the density is decreased.

The data clearly show a density threshold for the appearance of monoenergetic beams. Above $n_e = 2 \times 10^{19} \text{ cm}^{-3}$, monoenergetic electrons beams are consistently observed (close to 90% of shots). When the density is reduced below $n_e = 2 \times 10^{19} \text{ cm}^{-3}$, the monoenergetic electron beam appears more sporadically ($\approx 50\%$ of the time) and the dark current is also dramatically reduced.

Figure 2 summarizes the data presented in Fig. 1. It shows the variation of the electron beam energy with plasma density and the variation of the relative energy-spread of the electron beam. The curve is the linear (nonrelativistic) estimate for the maximum energy gain W_{\max} from the plasma wave due to dephasing.

At high electron number density ($n_e = 3 \times 10^{19} \text{ cm}^{-3}$) the monoenergetic beam energy is below w_{\max} , while for number densities in the range $n_e = (2-2.7) \times 10^{19} \text{ cm}^{-3}$, the beam energy is approximately W_{\max} . Below $n_e = 2 \times 10^{19} \text{ cm}^{-3}$, the beam energy is again lower than W_{\max} . At these lower densities, it is likely that the electrons have not reached the dephasing length; i.e., the interaction length was too short to reach the maximum energy W_{\max} . The (linear) dephasing length L_{dp} for $n_e = 1 \times 10^{19} \text{ cm}^{-3}$ is 1.85 mm, close to the entire length of the gas jet. Since there must be some evolution of the pulse (i.e., self-focusing and compression) before the wakefield reaches the point of self-injection, there is unlikely to be sufficient length in the 2 mm gas jet after injection, for the electron beam to reach the dephasing energy, W_{\max} .

The standard picture of self-injection in multidimensional nonlinear plasma waves is as follows: after the ponderomotive force of the laser pulse expels electrons at the front of the plasma wave bubble, electrons return laterally at the back of the bubble in response to the charge imbalance. In the wave frame, electrons that have low longitudinal velocity are injected at the rear of the bubble. Those electrons

that are injected first are accelerated ahead of those injected last until they reach the front of the plasma wave and are dephased. At this point, the tail of the bunch approaches the same energy as the head of the bunch. In this simple model, one would expect the energy-spread to be minimized when the electron beam energy is close to the dephasing energy. For this simple model to remain valid requires that the plasma wave electric field strength is constant over the duration of injection. The plasma wave amplitude can be affected by beam loading and laser pulse evolution. Simulations and experimental evidence⁶ show that the electron bunch is less than a plasma wavelength in length ($< 25 \text{ fs}$), and simulations show that significant pulse evolution occurs over many $1/\omega_p$. It is therefore unlikely that the change in the wakefield amplitude due to pulse evolution is the cause for the observed increase in the beam energy spread as the beam energy approaches W_{\max} .

Beam loading, i.e., the flattening of the laser wake due to the space charge of the electron bunch, will be more significant at higher densities, since the accelerated bunch has more charge, but beam loading is also unlikely to lead to increased energy spread. Once the plasma wakefield reaches the threshold for self-injection, electrons are continuously injected into the wave. The major effect of beam loading is to lower the electric field at the back of the bubble. If there is any significant lowering of the electric field then trapping can no longer occur. The cessation of trapping leads to narrow-energy-spread, short duration electron bunches. The flattening of the wake electric field due to beam loading results in the maximum energy of electrons injected later being lower than the maximum energy of those injected earlier. This may result in some increase in the energy spread but is unlikely to lead to the very large energy spreads observed when the beam energy approaches W_{\max} . This suggests an additional mechanism is causing longitudinal energy spread in the accelerated electron bunch.

It has been shown experimentally and in simulations that the interaction of the injected electrons and the laser field leads to an increase in the transverse emittance of the electron bunch.⁶ This effect is greater at high densities due to the increased overlap between the electron bunch and laser field. An alternative explanation for the increased energy spread observed in these experiments when $W \approx W_{\max}$ is that the interaction with the laser field increases the longitudinal emittance. The increase in transverse emittance is simply due to the extra transverse momentum electrons gain from the laser electric field. To explain an increase in longitudinal emittance due to the overlap between the electron bunch and the laser pulse requires that there is some direct laser acceleration occurring. At high densities the overlap between the laser pulse and the electron bunch at the back of the first plasma wave period is greater than at lower densities because at high density the laser occupies more of the first plasma wave period. The requirements for a direct laser acceleration (DLA) mechanism, such as that described in Ref. 9, are that there is an electron bunch, a transverse focusing force, and an intense laser field. These are clearly present in the situation described and an overlap between the electron bunch and the laser field (i.e., at high density) should result in some

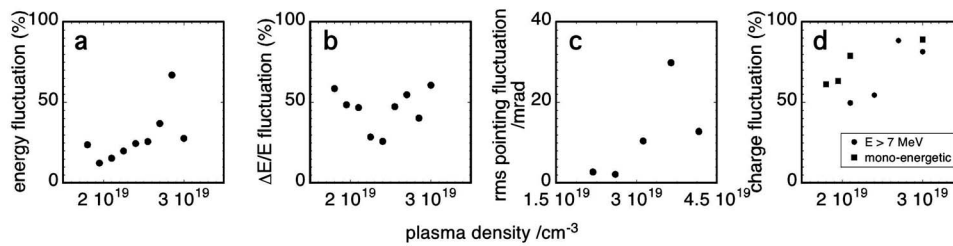


FIG. 3. Fluctuation of electron beam parameters as a function of plasma densities. (a) Standard deviation of electron beam peak energy (σ_W/\bar{W}). (b) Standard deviation of relative energy-spread [$\sigma_{\Delta W/W}/(\Delta W/\bar{W})$]. (c) Root mean square pointing fluctuation [$\sqrt{(\theta-\bar{\theta})^2}$]. (d) Standard deviation of electron charge as measured in the monoenergetic peak on the electron spectrometer (black squares) and as measured with a beam profile monitor for $W > 7$ MeV (gray circles) (σ_C/\bar{C}).

DLA. The acceleration of the bunch will still be dominated by the plasma wave electric field, but the DLA mechanism should act to increase the longitudinal emittance (i.e., energy spread) of the bunch.

Figure 3 shows the variation with density of the fluctuations in the principal beam parameters, specifically the energy, relative energy-spread, pointing, and charge. Each point on these graphs represents the standard deviation in the beam parameter from at least five measured electron spectra. There are some clear trends with density. The electron beam energy is significantly more stable at low densities exhibiting a standard deviation of 12% from its mean value [Fig. 3(a)]. However the shot-to-shot variation in energy-spread of the electron beam $\Delta W/W$ shows no obvious trend with density [Fig. 3(b)]. The relative energy-spread fluctuates by approximately 50% for all the densities investigated.

The beam pointing fluctuation, expressed as the root mean squared angular deviation from the mean position of the beam, shows a strong trend with density, with the stability increasing at lower densities [Fig. 3(c)]. The most stable beams showed fluctuations in pointing of 6 mrad. The beam charge also shows a trend of increasing stability with decreasing density. Figure 3(d) shows two sets of data recorded on different data runs. One set shows the fluctuation in the total charge of the beam as measured using the integrated signal on a beam profile monitor (for electrons with $W > 7$ MeV). The second set of data shows the fluctuations in the charge contained in the monoenergetic peak in the electron spectrometer, which shows that there is an appreciable variation in the charge in the accelerated beam, even in the best case ($>50\%$). Because the pointing stability and beam divergence are on the same order as the acceptance angle of the electron spectrometer, there is a coupling between pointing and charge stability. This explains why the fluctuations in the charge in the monoenergetic beam on the spectrometer are greater than the fluctuations of the whole beam profile.

The experimental data clearly show that the most stable beams were achieved at the lower densities close to $n_e = 2 \times 10^{19} \text{ cm}^{-3}$. At this density, the plasma wavelength is $7.6 \mu\text{m}$. It has been demonstrated experimentally and in simulations¹⁰ that self-focusing of an ultrashort pulse occurs until the pulse beam diameter (FWHM) reaches a stable value. In this regime ($a_0 \sim 1$), the stable value is on the order of the plasma wavelength λ_p . Since the (diffraction limited) vacuum focal spot is approximately $8 \mu\text{m}$, it is clear that the

lowest density corresponds to the closest to a matched spot. At higher densities, where the matched spot size is smaller, a greater degree of self-focusing must occur before the matched spot size is reached and this will lead to a greater degree of instability. The same is true when considering pulse compression and self-modulation of the pulse. At the highest density ($n_e = 3 \times 10^{19} \text{ cm}^{-3}$), the ratio of pulse length to plasma wavelength ($c\tau/\lambda_p$) is 1.7. At $n_e = 2 \times 10^{19} \text{ cm}^{-3}$, $c\tau/\lambda_p$ is closer to unity. Since pulse evolution also occurs in a plasma wave until $c\tau/\lambda_p < 1$ due to a combination of photon acceleration (and deceleration) and group velocity dispersion, the less the initial pulse length, the less evolution will be required. These data suggest that the instabilities in the electron beam parameters result from the period of pulse evolution occurring before injection. Hence, using a matched pulse with sufficient intensity to inject electrons immediately upon entry into the plasma would mitigate some of the sources of instability present in the current generation of self-injecting laser wakefield accelerators.

III. THRESHOLD FOR GENERATION OF MONOENERGETIC ELECTRON BEAMS

A characteristic of these experiments is a density threshold for the production of monoenergetic electron beams. Above this threshold, monoenergetic electron beams are produced consistently. At a plasma density of $n_e = 2.0 \times 10^{19} \text{ cm}^{-3}$, 89% of 27 shots showed monoenergetic electron beams. Just below this density, at $n_e = 1.8 \times 10^{19} \text{ cm}^{-3}$ only 50% of eight shots showed monoenergetic electrons beams. When the density was decreased further to at $n_e = 1.5 \times 10^{19} \text{ cm}^{-3}$, no energetic electrons were detected (0% of 10 shots).

This threshold is due to the fact that below a certain density the laser energy is too low to drive the wakefield to the point where injection of electrons occurs, even after pulse compression. The laser pulses used in these experiments are not sufficiently intense to drive the plasma wave to the point of injection immediately upon entry into the plasma. Instead, the production of electron beams relies on pulse evolution, i.e., self-focusing and compression, which occurs due to the refractive index gradients in the plasma wave. As the pulse becomes more intense, it is capable of driving a higher-amplitude plasma wave, which has steeper refractive index gradients and thus leads to further pulse focusing and com-

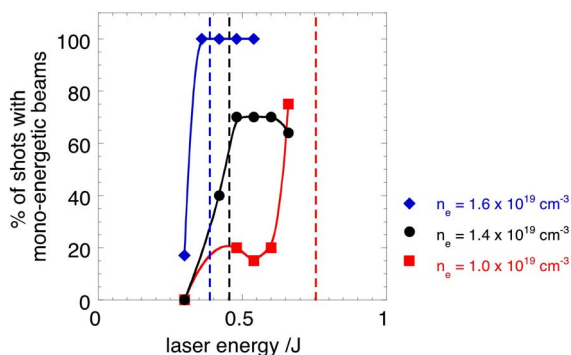


FIG. 4. (Color online) Percentage of shots showing monoenergetic spectra as a function of laser energy for three plasma densities. Diamonds: $n_e = 1.0 \times 10^{19} \text{ cm}^{-3}$; circles: $n_e = 1.4 \times 10^{19} \text{ cm}^{-3}$; squares: $n_e = 1.0 \times 10^{19} \text{ cm}^{-3}$. Dotted lines represent $\mathcal{E}_{\text{threshold}}$ for a threshold vector potential of $a_{\text{threshold}} = 3.2$.

pression. This positive feedback process continues until saturation, which occurs when the pulse has dimensions on the order of $w_{\text{FWHM}} = \lambda_p$ (see Ref. 10) and $c\tau_{\text{FWHM}} = \lambda_p/2$.¹¹ The density threshold for electron production with a given initial laser energy therefore occurs because there will be some density below which the intensity of the matched pulse will be insufficient to drive the wakefield to the point where injection occurs.

To investigate the effect of this phenomenon on the observed density threshold, the laser energy was varied for a number of fixed densities. In this experiment the plasma density was calculated from the frequency of Raman satellites present in the transmitted laser spectrum when a deliberately lengthened pulse was incident on the gas jet just prior to each set of data. This *in situ* measurement system was developed to monitor degradation in the jet density profile due to wear in the gas jet solenoid. In Fig. 4, the percentage of shots that show monoenergetic spectra as a function of laser energy is plotted for three different densities. Each curve in Fig. 4 shows behavior consistent with the threshold argument described above. At the highest density of $n_e = 1.6 \times 10^{19} \text{ cm}^{-3}$, the threshold is the most pronounced and occurs at the lowest laser energy, in the range $0.30 < \mathcal{E}_{\text{threshold}}/J < 0.36$. At this density, the monoenergetic electron beams were seen on 100% of five shots. Evidently, at this density, the laser is compressed to the smallest volume and therefore will achieve the highest intensity once it reaches the matched pulse width and duration. At $n_e = 1.4 \times 10^{19} \text{ cm}^{-3}$, the threshold behavior is still present, with 70% of 10 shots showing a monoenergetic spectrum. At this density, the threshold occurs in the range $0.30 < \mathcal{E}_{\text{threshold}}/J < 0.5$. At the lowest density ($n_e = 1.0 \times 10^{19} \text{ cm}^{-3}$), the stability increases with increasing laser energy, although a stable plateau has not been reached by $\mathcal{E}_{\text{laser}} = 0.68 \text{ J}$.

We note that the observed thresholds in this data set occur at slightly lower densities than in the initial data set presented in Fig. 1. This is likely due to a better optimized gas flow from the gas jet in the second set of data. The electron beam energies in this data set were also higher, close to $W = 140 \text{ MeV}$ [$W_{\text{max}} \approx 180\text{--}110 \text{ MeV}$ in the range $n_e = (1.0\text{--}1.8) \times 10^{19} \text{ cm}^{-3}$] consistent with this data set being

at a lower plasma density than the data in Fig. 1. An improved optimization of the neutral gas probably results in a shorter density scale length at the edges of the gas flow which may promote injection at lower densities. The interaction of the laser pulse with the $100 \mu\text{m}$ scale density ramp complicates the pulse evolution stage of the interaction and may effect, for example, pump depletion or the amount of laser energy trapped in the self-focused filament. This demonstrates that the exact gas profile is important in determining the parameters (or threshold) for self-injection and indicates that control of the density profile may be a useful method of controlling the self-injection process.

Using a simple model we can estimate the threshold vector potential required for electron injection. The laser power is related to the spot size and plasma wavelength by

$$\frac{P_L}{P_c} \approx \frac{\pi^2}{8} a_0^2 \frac{w_0^2}{\lambda_p^2}, \quad (1)$$

where $P_c = 17.3 n_c/n_e \text{ GW}$ is the critical power for self-focusing, w_0 is the beam waist, and a_0 is the peak normalized vector potential of the laser field. For a Gaussian temporal profile, the pulse duration τ [fs] is related to the peak power by $P_L \approx 0.92 \mathcal{E}_L / \tau_{\text{FWHM}}$ [GW]. If we assume that the compressed pulse waist tends towards λ_p , and the pulse duration towards $\tau_{\text{FWHM}} = \lambda_p/2$ and that all of the initial laser energy is compressed, an expression can be obtained for the threshold laser energy for self-injection:

$$\mathcal{E}_{\text{threshold}} = 23.3 \times 10^9 \left(\frac{n_c}{n_e} \right) a_{\text{threshold}}^2 \tau_{\text{FWHM}} [\text{J}]. \quad (2)$$

Treating the vector potential threshold $a_{\text{threshold}}$ as a free parameter, the observed energy thresholds can be fitted to the model using a least-squares method. The predicted values are shown as dotted lines in Fig. 4. Assuming 100% of the initial laser energy is compressed leads to a best fit for $a_{\text{threshold}} = 3.2$. These values are consistent with the observed trends in two-dimensional (2D) and three-dimensional (3D) particle-in-cell (PIC) simulations.¹² This simplified model does not include the following factors: frequency shifts can strongly affect the vector potential; similarly, the fraction of energy trapped and compressed is not likely to be constant over a wide range of densities. In particular, at higher densities, it is unlikely that all of the laser energy will be trapped in a single filament.¹⁰ Nevertheless, the model does provide direct experimental evidence that normalized vector potentials $a_0 \gtrsim 3$ are required in a matched pulse for self-injection to occur. For a multidimensional treatment of nonlinear plasma waves, the matched pulse waist is given by $w_0 = \sqrt{2} a_0 c / \omega_p$.¹³ Assuming a Gaussian profile with $a_{\text{threshold}} \approx 3.2$, this expression becomes $w_{\text{FWHM}} \approx 5.3 c / \omega_p$, similar to the observed matched spot size.¹⁰

IV. DISCUSSION

This paper reports a study into the stability of single beam self-injection laser wakefield accelerators. The stability achieved on the Lund multi-terawatt laser system is, in terms of the principal electron beam parameters of energy, energy-

spread, pointing, and charge, an order of magnitude better than achieved in the first proof-of-principle experiments on the Astra laser.²

These beams are now of suitable reproducibility for detailed investigations of beam characteristics. For example, it has been possible to effectively cross-correlate the laser field with the electron bunch. In so doing, the injection dynamics have been verified and the ultrashort duration of the electron bunch demonstrated.⁶

It is noted that the laser energy was approximately the same in the two experiments. The major differences between the present experiments and the first experiments are a shorter pulse duration (35 fs compared with 45 fs) and tighter focusing ($f/10$ compared with $f/16$). Both factors result in the laser pulse being initially closer to the matched parameters in the present study, especially the spot size. This is emphasized by the experimentally determined density dependence, which demonstrates an enhanced stability at lower plasma densities, for which the pulse is most closely matched to the ideal dimensions.

Another important factor is the contrast ratio. For the present investigations, the contrast ratio $I_0/I_{\text{ASE}}=10^8$ as compared with 10^6 previously. This has also been demonstrated to improve the observed stability.¹⁴

The experimental results are also consistent with a threshold intensity required for self-injection, corresponding to a normalized vector potential in the matched pulse of $a_0 \approx 3$. This is consistent with theoretical calculations for the intensity threshold for transverse self-injection into a 3D plasma wave.¹³

Many of these results are of important consequence for future laser plasma acceleration experiments. For the next generation of ultrashort petawatt class lasers, it should be possible to introduce the pulse into the plasma with a matched pulse width of sufficient intensity to initiate self-injection immediately. For example the Astra Gemini laser, currently under development at the Rutherford-Appleton Laboratory, which will have a pulse energy of $\mathcal{E}_L=15$ J and pulse duration of $\tau=30$ fs. One of the experimental configurations available will be $f/20$ focusing. The focal spot in this configuration will be $w_0 \approx 20$ μm , which will be close to matched at a plasma density $n_e=2 \times 10^{18}$ cm^{-3} . The linear dephasing energy and length at this density are $W_{\text{max}}=0.85$ GeV and $L_{\text{dp}}=19$ mm. Since the matched pulse is stable to diffraction and focusing it is reasonable to expect that self-guiding over this range will be achievable. To investigate this we have performed a centimeter scale simulation of the long focal length configuration, close to the matched density. The simulation presented was on a grid 204×204 μm with a resolution of 30 cells per laser wavelength in $x-ct$, the propagation direction, and 7.9 cells per laser wavelength in the transverse direction y . The laser was polarized in the slab. Figure 5(a) shows the electron density profile after the laser has propagated for 9 mm. There is a clear plasma wave bubble and electrons have been injected into the first plasma wave period. The laser spot was close to matched, oscillating slightly about the matched spot size. This is shown in Fig. 5(b) as a time history of the integrated transverse laser intensity profile. The oscillation period is

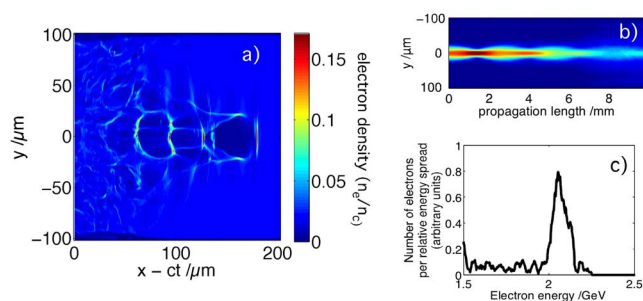


FIG. 5. (Color online) Results from a 2D PIC simulation with OSIRIS for the Astra Gemini system. $\mathcal{E}_L=10$ J, $\tau=30$ fs, $w_0=20$ μm , $a_0=4.8$, $n_e=2 \times 10^{18}$ cm^{-3} . (a) Electron density profile after the laser has propagated 9 mm. (b) Laser transverse intensity profile (integrated along $x-ct$) as a function of propagation distance. (c) Electron energy spectrum after 9 mm propagation.

close to 2 mm, on the same order as the Rayleigh range $Z_R=1.57$ mm. After propagating 9 mm, the laser has undergone significant pump depletion and pulse etching. The electron energy spectrum at this point is shown in Fig. 5(c). In this 2D simulation the beam has reached 2 GeV with an energy spread of a few percent. This is close to, but significantly higher than, the basic linear prediction of 0.85 GeV, indicating that the simple scaling law needs to be modified for high initial laser intensities.

In summary, we have observed the production of quasi-monoenergetic electron beams from a 20 TW laser system. We find that the stability of the electron beam is significantly improved for plasma densities that correspond to the laser pulse being matched to the wakefield dimensions. It was the improved electron beam stability that led directly to the ability to perform experiments into the electron trapping dynamics as reported in Ref. 6. We have observed an energy-density threshold for the stable production of monoenergetic electron beams. This threshold is consistent with the model that the laser is compressed in time and space to dimensions on the order of λ_p , and that injection occurs when there is an intensity corresponding to $a_0 \gtrsim 3$ in this matched spot. Matching reduces the amount of evolution required before injection occurs and indicates that stability may be improved further if the laser is sufficiently intense to inject electrons into the wake without evolution.

ACKNOWLEDGMENTS

We acknowledge support from the Swedish Research Council, the Knut and Alice Wallenberg foundation, the EU Access to Research Infrastructures Programme (RII3-CT-2003-506350 Laserlab Europe) and Research Councils UK.

¹W. P. Leemans, B. Nagler, A. J. Gonsalves *et al.*, Nature (London) **2**, 696 (2006).

²S. P. D. Mangles, C. D. Murphy, Z. Najmudin *et al.*, Nature (London) **431**, 535 (2004).

³C. G. R. Geddes, C. Toth, J. v. Tilborg *et al.*, Nature (London) **431**, 538 (2004).

⁴J. Faure, Y. Glinec, A. Pukhov *et al.*, Nature (London) **431**, 541 (2004).

⁵S. Fritzler, E. Lefebvre, V. Malka *et al.*, Phys. Rev. Lett. **92**, 165006 (2004).

- ⁶S. P. D. Mangles, A. G. R. Thomas, M. C. Kaluza *et al.*, Phys. Rev. Lett. **96**, 215001 (2006).
- ⁷A. I. Akhiezer and R. V. Polovin, Zh. Eksp. Teor. Fiz. **30**, 915 (1956).
- ⁸A. Pukhov and J. Meyer-ter Vehn, Appl. Phys. B: Lasers Opt. **74**, 355 (2002).
- ⁹A. Pukhov, Z. M. Sheng, and J. Meyer-ter Vehn, Phys. Plasmas **6**, 2847 (1999).
- ¹⁰A. G. R. Thomas, Z. Najmudin, S. P. D. Mangles *et al.*, Phys. Rev. Lett. **98**, 095004 (2007).
- ¹¹J. Faure, Y. Glinec, J. J. Santos *et al.*, Phys. Rev. Lett. **95**, 205003 (2005).
- ¹²F. S. Tsung, W. Lu, M. Tzoufras *et al.*, Phys. Plasmas **13**, 056708 (2006).
- ¹³W. Lu, C. Huang, M. Zhou *et al.*, Phys. Rev. Lett. **96**, 165002 (2006).
- ¹⁴S. P. D. Mangles, A. G. R. Thomas, M. C. Kaluza *et al.*, Plasma Phys. Controlled Fusion **48**, B83 (2006).